Long-lived period-doubled edge modes of interacting and disorder-free Floquet spin

Daniel J. Yates¹, Alexander G. Abanov^{2,3}, and Aditi Mitra¹

¹Center for Quantum Phenomena, Department of Physics,
New York University, 726 Broadway, New York, NY, 10003, USA

²Simons Center for Geometry and Physics, Stony Brook, NY 11794, USA

³Department of Physics and Astronomy, Stony Brook University, Stony Brook, NY 11794, USA

(Dated: February 4, 2022)

ABSTRACT

Floquet spin chains have been a venue for understanding topological states of matter that are qualitatively different from their static counterparts by, for example, hosting π edge modes that show stable period-doubled dynamics. However the stability of these edge modes to interactions has traditionally required the system to be many-body localized in order to suppress heating. In contrast, here we show that even in the absence of disorder, and in the presence of bulk heating, π edge modes are long lived. Their lifetime is extracted from exact diagonalization and is found to be non-perturbative in the interaction strength. A tunneling estimate for the lifetime is obtained by mapping the stroboscopic timeevolution to dynamics of a single particle in Krylov subspace. In this subspace, the π edge mode manifests as the quasi-stable edge mode of an inhomogeneous Su-Schrieffer-Heeger model whose dimerization vanishes in the bulk of the Krylov chain.

INTRODUCTION

Periodically driven or Floquet systems are promising venues for identifying states of matter that do not exist in thermal equilibrium [1]. Perhaps the most striking among these athermal states are Floquet systems with new topological properties and bulk boundary correspondences that require defining new topological invariants [2, 3]. For example, while a static two-band system may be characterized by an integer \mathbb{Z} valued or a \mathbb{Z}_2 valued topological invariant [4-6], two-band free fermion Floquet systems require at least one more topological invariant so that the system has a $\mathbb{Z} \times \mathbb{Z}$ or a $\mathbb{Z}_2 \times \mathbb{Z}_2$ classification [7–9]. The additional topological invariant arises due to the periodic nature of the Floquet spectrum. In particular, since the energy in a periodically driven system is conserved only up to integer multiples of the drive frequency Ω , one has quasi-energy bands rather than energy bands. These quasi-energy bands span a Floquet Brillouin zone (FBZ), $\epsilon \in [-\Omega/2, \Omega/2]$, with the boundaries of the FBZ being continuous. The additional topological invariant characterizes edge modes that can reside at the zone boundaries $\epsilon = \pm \Omega/2$.

For two dimensional systems, the additional topological invariant leads to the anomalous Floquet insulator

where a bulk has zero Chern number, yet chiral edge modes propagate at the boundary [10–13]. For one dimensional (1d) systems, the edge modes that reside at the Floquet zone boundary are known as π edge modes [14–16]. Since these modes have a periodicity which is twice that of the drive period, they are examples of boundary time crystals [17–19]. Of course, the $\mathbb{Z} \times \mathbb{Z}$ or a $\mathbb{Z}_2 \times \mathbb{Z}_2$ classification implies that 0 and π edge modes can exist separately, or together, leading to a rich phase diagram [20–23].

The π edge modes occurring in most 1d systems [14–16, 24] also have their origin in what are known as strong π modes (SPM) [25], whose precise definition we now give. Denoting the π strong mode as Ψ_{π} , these are operators that have the property that they anti-commute with a discrete, say \mathbb{Z}_2 symmetry, which we denote by \mathcal{D} . Thus, $\{\Psi_{\pi}, \mathcal{D}\}=0$. In addition, the SPM anti-commutes with the Floquet unitary U that generates stroboscopic timeevolution, $\{\Psi_{\pi}, U\} \approx 0$. The symbol \approx is to represent the fact that the anti-commutation is strictly speaking obeyed only in the thermodynamic limit. For a finite size system of length L, $\{\Psi_{\pi}, U\} \propto |u|^L$, where |u| < 1, so that the anti-commutator is suppressed exponentially in the system size. The third feature of the SPM is that it is a local operator with the property $\Psi_\pi^2 = O(1)$. The existence of a SPM implies an eigenspectrum phase where each eigenstate $|n\rangle$ of a certain parity has a pair $\Psi_{\pi}|n\rangle$ of the opposite parity, with the quasi-energies of the two states separated by π/T , where $T=2\pi/\Omega$ is the period of the drive. Note that the above definition of SPMs can be generalized to more complex $2\pi/k$ edge modes where k is an integer [26].

When interactions are included, these operators no longer exactly anti-commute with U in the thermodynamic limit, and therefore acquire a lifetime. Yet a fascinating aspect of these edge modes, which is the central topic of this paper, is that the lifetime far exceeds bulk heating times [25]. These quasi-stable edge modes that almost, rather than exactly anti-commute with U, are referred to as almost strong π modes (ASPM). When disorder is present, the expectation is that many-body localization will make the SPM stable to interactions at all times [20, 27–31]. This paper, in contrast, concerns the stability of π modes for disorder-free chains, and determines how their lifetime depends on interactions. There are of course other contexts, besides ASPMs, where disorder-free Floquet systems can be stable to interac-

tions for long times [32–37].

An analogous definition exists for a strong zero mode (SZM) Ψ_0 [38–41]. This is a local operator that obeys all the above properties except that Ψ_0 commutes with the Floquet unitary in the thermodynamic limit $[\Psi_0, U] \approx 0$. Thus existence of a SZM implies an eigenspectrum phase where the entire spectrum of U is at least doubly degenerate. Adding interactions makes the SZM into a quasistable almost strong zero mode (ASZM). Since SZMs and ASZMs have by now been discussed in detail in static systems [42–47], in this paper we will only focus on SPMs and ASPMs. A central goal of this paper is to establish how the lifetime of the π mode depends on interactions. In the process we present Krylov time-evolution as a tool for studying Floquet dynamics. This approach has so far only been employed for static Hamiltonians [46–50]. Here we show how Krylov techniques can be used to extract tunneling times of quasi-stable modes of driven systems.

We will study the stroboscopic dynamics of an open spin-1/2 chain of length L. The dimension of the Hilbert space of the problem is 2^L . The natural numerical method of choice is exact diagonalization (ED), and we are limited to a system size of L=14. Since we are interested in extracting lifetimes in the thermodynamic limit of $L\to\infty$, ED can be restrictive, and alternate numerical and analytical methods are needed. Thus the results presented here, besides being an explication of the unusual physics of ASPMs, also provide a roadmap for developing methods for understanding slow, system size independent dynamics.

RESULTS AND DISCUSSION

Model: We will study an open chain of length L whose stroboscopic time-evolution is generated by the following Floquet unitary

$$U = e^{-i\frac{T}{2}J_z H_{zz}} e^{-i\frac{T}{2}J_x H_{xx}} e^{-i\frac{T}{2}gH_z},$$
(1)

where

$$H_z = \sum_{i=1}^{L} \sigma_i^z; H_{xx} = \sum_{i=1}^{L-1} \sigma_i^x \sigma_{i+1}^x; H_{zz} = \sum_{i=1}^{L-1} \sigma_i^z \sigma_{i+1}^z.$$
(2)

Above $\sigma^{x,y,z}$ are the Pauli matrices, and in what follows we set $J_x = 1$. Eq. (1) is an example of a ternary drive where during one period, a magnetic field of strength Tg is applied, followed by the application of a nearest neighbor exchange interaction of strength T along the x direction, and this is followed by the application of a nearest neighbor exchange interaction of strength TJ_z along the z-direction. The Floquet unitary has a discrete symmetry as it commutes with $\mathcal{D} = \sigma_1^z \dots \sigma_L^z$.

When $J_z = 0$, the model can be mapped to free fermions through a Jordan-Wigner transformation. In this free limit any operator can be expanded in a basis

of 2L Majorana fermions or Pauli string operators. Thus when $J_z=0$, the dimension of the space needed to diagonalize the problem is only 2L rather than the dimension of the full Hilbert space 2^L . The existence of this free limit has been valuable for identifying strong modes. In fact, at the special point of $Tg=\pi$, the Floquet unitary for $J_z=0$ reduces to $U=(-i)^L\mathcal{D}e^{-i\frac{T}{2}J_xH_{xx}}$ [20]. At this special point, the SPM is simply the Pauli spin operator on the first site $\Psi_\pi=\sigma_1^x$. It is straightforward to check that σ_1^x has all the properties of a SPM as summarized in the Introduction. It is a local operator with $\Psi_\pi^2=1$, it anti-commutes with \mathcal{D} , and it anti-commutes with U. Even away from this special point, although the SPM is a more complex operator, it continues to have the property that it has a non-zero overlap with σ_1^x [15, 25].

Including interactions, i.e, $J_z \neq 0$, as anticipated in the Introduction, the SPM changes to an ASPM. Moreover, this operator continues to have an overlap with σ_1^x for weak interactions. Therefore, an efficient way to determine whether the system hosts these special edge modes is through the study of the following autocorrelation function

$$A_{\infty}(nT) = \frac{1}{2^L} \operatorname{Tr} \left[\sigma_1^x(nT) \sigma_1^x(0) \right], \tag{3a}$$

$$\sigma^x(nT) = \left[U^{\dagger}\right]^n \sigma_1^x U^n. \tag{3b}$$

We only study the dynamics at stroboscopic times, so n is an integer. Moreover, A_{∞} is an infinite temperature average as the trace is over the entire Hilbert space. Thus this quantity is a highly out of equilibrium measure of the system dynamics. When an ASPM or an ASZM is non-existent or if we replace σ_1^x by an operator deep in the bulk of the chain, A_{∞} will decay to zero within a few drive cycles. Throughout this paper, all numerical results will be for g=0.3 and T=8.25, but for different values of J_z . For this value of g, T, when $J_z=0$ we have a SPM. When J_z is non-zero, the SPM changes to an ASPM.

Exact Diagonalization (ED): We first present results for the stroboscopic time-evolution of A_{∞} from ED. Fig. 1 plots A_{∞} for $J_z = 0.01$, for three different system sizes L = 6, 8, 10. The x-axis which denotes the stroboscopic times is on a logarithmic scale. One finds that A_{∞} flips sign between neighboring stroboscopic times, thus we have an ASPM. Moreover, for small system sizes, as L increases, the lifetime of the ASPM increases (compare L=6 with L=8 in the figure), but eventually the lifetime reaches a system size independent value. For the chosen parameters, the system size independent lifetime is reached by L = 8 as the plots for L = 8 and L=10 nearly coincide. We refer to this system size independent lifetime as the lifetime in the thermodynamic limit. Moreover, for $J_z = 0.01$, this lifetime is around 10⁴ drive cycles. Note that the high frequency limit requires $T \ll 1$, and since we have T = 8.25, we are far from the high frequency limit. Thus, the bulk is in fact heating, as expected for a periodically driven interacting,

and disorder-free system [51–55]. The evidence from ED for bulk heating was already presented in Ref. 25, where it was shown that the autocorrelation function for bulk operators decays to zero within a few drive cycles, and that the entropy density rapidly approaches the maximum possible value (accounting for finite size effects). Further below we discuss the signature of bulk heating in Krylov subspace. We also extend the results of Ref. 25 by extracting the interaction dependence of the lifetime of the π -mode using several different approaches: ED, Krylov dynamics, and domain wall counting.

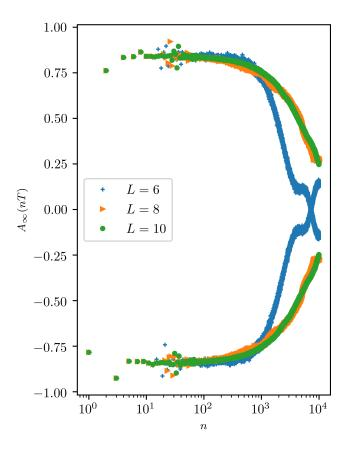


FIG. 1. System size dependence of the autocorrelation function. The autocorrelation function A_{∞} at stroboscopic times nT, where T is the drive period, and n is an integer. The results are for a magnetic field of strength g=0.3, interaction of strength $J_z=0.01$, and period T=8.25, for three different system sizes L=6,8,10. The x-axis is on a logarithmic scale. The system hosts an almost strong π mode (ASPM) as is clearly visible by the flipping of the sign of A_{∞} between neighboring stroboscopic times. For these parameters the ASPM decays at the same time for L=8 and L=10. Thus the thermodynamic limit for the lifetime is already reached for L=8, with this lifetime being approximately 10^4 drive cycles.

We now discuss how the lifetime in the thermodynamic limit depends on J_z . Fig. 2 shows the autocorrelation function accounting for its period-doubled behavior $A_{\infty}^p(nT) = (-1)^n A_{\infty}(nT)$. Since the sign-flipping of

 A_{∞} is absorbed by the $(-1)^n$ factor, A_{∞}^p has a smoother behavior in time. We plot A_{∞}^p for different J_z and for system sizes L=8,10,12,14. The smallest possible J_z we can study is $J_z=0.001$ because for J_z values smaller than this, the system size needed for the lifetime to become L independent, is larger than L=14. While the stroboscopic times in Fig. 1 were linearly separated, the stroboscopic times in Fig. 2 are logarithmically separated as the lifetimes increase dramatically with decreasing J_z , and linearly separated points are numerically too costly to compute.

Fig. 2 clearly shows that as J_z increases (panels (a-g)), the lifetime of the ASPM decreases. In fact the thermodynamic lifetimes are already reached for L=8 when $J_z=0.01$ as the plots for all the four system sizes lie on top of each other (panel (g)). Recall that Fig. 1 is a more detailed version of A_∞ for precisely this value of J_z , where the stroboscopic times are linearly separated, and one smaller system size, L=6, is shown in order to highlight the system size dependence.

We employ the ansatz that $A^p_{\infty}(nT) = e^{-\Gamma nT} A^p_{\infty}(n_0T)$, where we choose $n_0 = 10$ as it takes about 10 drive cycles for the initial transients to decay. The decay rate Γ is extracted from determining the time at which $A^p_{\infty}(\Gamma^{-1}) \approx e^{-1} A^p_{\infty}(10T)$. This ansatz is plotted in Fig. 2 and captures the time-evolution very well. The decay rates Γ are plotted in Fig. 3 where now it is the y-axis that is plotted on a logarithmic scale. The almost linear slope for $1/J_z \gg 1$ suggests that (restoring J_x)

$$\Gamma \sim e^{-cJ_x/J_z}$$
. (4)

Above c is a O(1) number that depends on g, J_x . Thus for small enough J_z , ED indicates that the decay rates are non-perturbative in the strength of the interactions J_z . As J_z is further increased, we do not expect the edge mode to be an ASPM, and its decay rate will be determined entirely by perturbative processes $\Gamma \propto O(J_z^{\alpha})$, where α is a power of O(1).

Krylov subspace dynamics: In order to understand the origin of the non-perturbatively long lifetimes for $J_z \ll 1$, and its relation to bulk heating, we map the stroboscopic time-evolution of σ_1^x to dynamics of a free particle in a Krylov subspace employing a recursive Lanczos scheme [48–50, 56, 57]. This mapping to single particle physics will allow us to develop a tunneling picture for the lifetime of the ASPM.

Let us define the Floquet Hamiltonian as $H_F = i \ln(U)/T$. The stroboscopic time-evolution after m periods of a Hermitian operator O can be written in terms of H_F as follows

$$\left[U^{\dagger}\right]^{m}OU^{m} = e^{iH_{F}mT}Oe^{-iH_{F}mT} = \sum_{n=0}^{\infty} \frac{(imT)^{n}}{n!} \mathcal{L}^{n}O,$$
(5)

where we define $\mathcal{L}O = [H_F, O]$. To employ the Lanczos algorithm, we recast the operator dynamics into vector

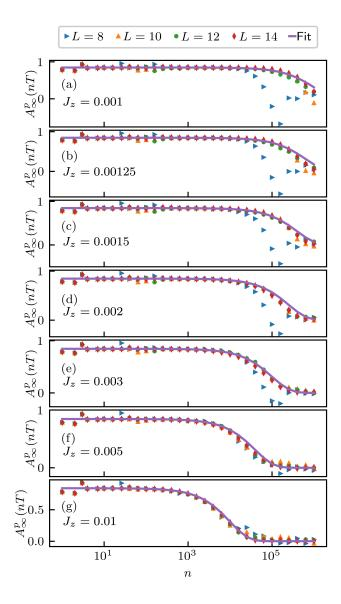


FIG. 2. Interaction and system size dependence of the autocorrelation function. The autocorrelation function accounting for the sign-change between neighboring strobosocopic times $A_{\infty}^p(nT)=(-1)^nA_{\infty}(nT)$ is plotted for stroboscopic and logarithmically separated times nT, where T is the period and n is an integer. The results are for a magnetic field of strength g=0.3, period T=8.25, and for different interaction strengths J_z . The x-axis is on a logarithmic scale. From panels (a-g) J_z increases. Panel (g) corresponds to $J_z=0.01$ and the corresponding time evolution for $A_{\infty}(nT)$ for linearly separated times is shown in Fig. 1. Also shown is a fit (purple line) to an exponential $A_{\infty}^p(nT)=e^{-\Gamma nT}A_{\infty}^p(10T)$, where Γ is a decay rate.

dynamics by defining $|O\rangle = O$. Since we are concerned with infinite temperature quantities, we have an unambiguous choice for an inner product on the level of the operators, $(A|B) = \text{Tr}\left[A^{\dagger}B\right]/2^{L}$. The Lanczos algorithm iteratively finds the operator basis that tri-diagonalizes \mathcal{L} .

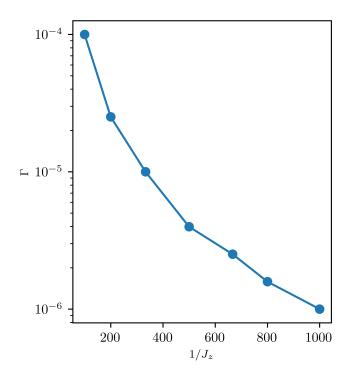


FIG. 3. Decay rates of the π mode extracted from exact diagonalization (ED). The decay rate from the ED data in Fig. 2 plotted on a logarithmic scale vs $1/J_z$ where J_z is the interaction strength. The constant slope for $1000 \ge 1/J_z \ge 500$ indicates that for $1/J_z \gg 1$, the decay rate is $\Gamma \approx e^{-c/J_z}$, where J_z is in units of J_x and c is a O(1) number.

We begin with the seed "state", $|O_1\rangle$, and let $\mathcal{L}|O_1\rangle = b_1|O_2\rangle$, where $b_1 = \sqrt{|\mathcal{L}|O_1\rangle|^2}$. The recursive definition for the basis operators $|O_{n\geq 2}\rangle$ is, $\mathcal{L}|O_n\rangle = b_n|O_{n+1}\rangle + b_{n-1}|O_{n-1}\rangle$, where we define $\bar{b}_{n\geq 2} = \sqrt{|\mathcal{L}|O_n\rangle - b_{n-1}|O_{n-1}\rangle|^2}$. It is straightforward algebra to check that the above procedure will yield a \mathcal{L} of the form

$$\mathcal{L} = \begin{pmatrix} b_1 & b_2 \\ b_2 & \ddots \\ & \ddots & \end{pmatrix}. \tag{6}$$

The basis spanned by $|O_n\rangle$ lies within the Krylov subspace of \mathcal{L} and $|O_1\rangle$. We refer to this tri-diagonal matrix as the Krylov Hamiltonian H_K , $H_K = \sum_n b_n (c_n^{\dagger} c_{n+1} + c_{n+1}^{\dagger} c_n)$, and the 1d lattice it represents, as the Krylov chain.

For free systems, the operation $\mathcal{L}|O_n$) can be efficiently solved in the Majorana basis. If the starting operator is a single Majorana, then the dimension of the Krylov subspace of that operator will scale as 2L, as free system dynamics can only mix the individual Majoranas among themselves. Outside of free problems, the size of the full set of $|O_n\rangle$ will be large. For example, a

system of size L will have $\sim 2^{2L}$ possible basis operators. Since we are interested in the thermodynamic limit for the lifetime of the edge operator, in what follows, we will treat the Krylov chain to be a semi-infinite chain. The Krylov chain of interest to us is the one where the seed operator $|O_1\rangle = |\sigma_1^x\rangle$. Then A_∞ is equivalent to $A_\infty(nT) = (e^{i\mathcal{L}nT})_{1,1}$. Thus the dynamics of A_∞ has been transformed into that of a semi-infinite, single-particle problem where $A_\infty(nT)$ is now the probability that a particle initially localized at the end of the Krylov chain, stays localized at the end at time nT.

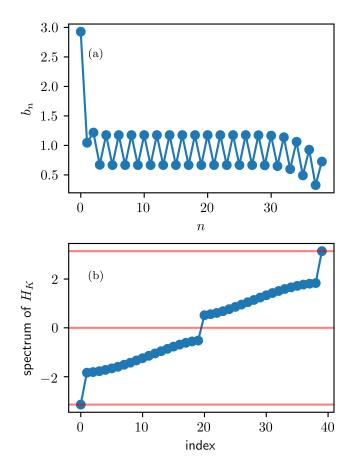


FIG. 4. Parameters of the Krylov chain for the free case. The hopping parameters b_n for the Krylov chain (panel (a)) and the corresponding spectrum (panel (b)) for the free case $J_z = 0$, where J_z is the interaction strength. The strength of the magnetic field is g = 0.3, the period T = 8.25, and the system size L = 20. n labels the sites of the Krylov chain. The horizontal red lines in panel (b) indicate energies at $0, \pm \pi$. Panel (b) shows modes at $\pm \pi$ that are clearly separated from bulk states by an energy gap.

As a point of orientation, let us discuss the details of the Krylov subspace in the free limit. In the Majorana basis, the stroboscopic time evolution of an operator $\vec{a} = [a_1, a_2, \dots a_{2L}]^T$ is (see Supplementary Note 1)

$$U^{\dagger} \vec{a} U = K \vec{a}, \tag{7}$$

where K is a $2L \times 2L$ orthogonal matrix and the a_i are Majoranas with $a_1 = \sigma_1^x$. For studying SM dynamics, our seed operator is $\vec{a} = [a_1, 0, 0, 0 \dots]^T$. The components of K can be determined analytically. On comparing equations (5) and (7), we identify the operator $iT\mathcal{L}$ with $\ln K$. Since \mathcal{L} is an operator, whose precise form depends on the basis, we have argued that the Krylov Hamiltonian H_K is related to $i \ln K$ by a simple basis rotation.

The form of $i \ln K$ becomes particularly simple close to the exactly solvable point $gT = \pi$ and in the high frequency limit $T \ll 1$. Denoting $s_1 = \sin(gT)$, in the first order in s_1 and T we find (see Supplementary Note 1)

$$i \ln K \approx \begin{pmatrix} 0 & is_1 & 0 & 0 & 0 & 0 \\ -is_1 & 0 & -iT & 0 & 0 & 0 \\ 0 & iT & 0 & is_1 & 0 & 0 \\ 0 & 0 & -is_1 & 0 & -iT & 0 \\ 0 & 0 & 0 & iT & 0 & is_1 \\ 0 & 0 & 0 & 0 & -is_1 & 0 \end{pmatrix} \pm \pi. \tag{8}$$

The analytic result in Eq. (8) shows that $i \ln K$ is like a Su-Schrieffer-Heeger (SSH) model [58, 59] with a topologically non-trivial dimerization for $|s_1| < T$. Moreover the overall shift of π ensures that the edge mode of the SSH model is pinned at π rather than at zero energy. The SSH model is a band insulator with a band-gap controlled by the strength of the dimerization $||s_1| - T|$. In contrast, when the dimerization is zero, the model is a trivial metal. We will see below that switching on interactions leads to inhomogeneities such that insulating regions of non-zero dimerization coexist with metallic regions of zero dimerization.

In the limit where Eq. (8) is valid, we can derive the Krylov Hamiltonian analytically (see Supplementary Note 1). We find that $b_{\rm odd} = |s_1|$, $b_{\rm even} = T$, with a constant term $\pm \pi$ along the diagonals. Thus when $|s_1| < T$, the Krylov Hamiltonian is a topologically non-trivial SSH model that hosts a zero mode. The constant term along the diagonal shifts its energy to π .

The b_n s for g = 0.3 and T = 8.25, and for the free case $J_z = 0$ are shown in Fig. 4(a). For this case, $|s_1|$ and T are no longer small. Thus there are differences in the Krylov parameters between this case, and the exact solution around $gT \approx \pi$ just discussed. One is that the Krylov Hamiltonian has zeros on the diagonals away from the exactly solvable limit. The second is that the hopping on the very first site is large. However, as suggested by the analytic form in the exactly solvable limit, the Krylov chain is a SSH model with a uniform dimerization after $n \gtrsim 4$. Fig. 4(b) shows the corresponding spectrum of the Krylov chain, where the three horizontal red lines are at $\epsilon = 0, \pm \pi$. Modes at $\pm \pi$ that are also separated from the bulk modes by a gap, are clearly visible. Thus we see that even though the diagonal term of the Krylov chain is zero, it is the initial large hopping of $b_1 \approx \pi$ that ensures that the edge modes of the SSH model are pinned at $\pm \pi$.

In fact the effective model for the Krylov chain for $J_z=0$ can be written as $H_K=H_{\rm SSH}+H_E$, where $H_{\rm SSH}$ represents a SSH model and captures the behavior from sites $n \gtrsim 4$, while H_E is an edge Hamiltonian that captures the physics on the first few sites. The SPM ψ_π is a zero mode of $H_{\rm SSH}$, while $H_E\psi_\pi=\pi\psi_\pi$. Thus $H_K\psi_\pi=\pi\psi_\pi$. To obtain a π edge mode, the parameters of H_E are finely tuned, while $H_{\rm SSH}$ only requires its dimerization to be topologically non-trivial to ensure a zero mode. The role of H_E is to raise the energy of the zero mode to π .

Note that this mapping from the Floquet unitary U to the Krylov chain has lost information about the periodic nature of the spectrum of U, and this manifests as finely tuned b_n at the edge of the Krylov chain when a π mode exists. Nevertheless this mapping to an effectively free model helps to arrive at a tunneling estimate for the lifetime of the π mode when interactions are non-zero. We discuss this below.

We now switch on interactions. We expect the dynamics to explore larger regions of the Hilbert space, resulting in more complicated b_n . These are shown in Fig. 5(b-e) for system size L=12 and with different J_z . Fig. 5(gj) show the corresponding spectra. For easy comparison between the free and interacting cases, Fig. 5(a,f) correspond to $J_z = 0$. The blue circles (all panels Fig. 5) correspond to carrying out the Lanczos procedure in the spin basis, which is the natural choice when interactions are present. In contrast, the free case involved performing Lanczos in the Majorana basis Fig. 5(a,f). The periodicity of U is lost in the Lanczos approach, and the resulting b_n are sensitive to the choice of the branch of ln(U). This leads to b_n s (blue circles Fig. 5(b-e)), which do not bear much of a resemblance to the b_n s of the free case Fig. 5(a), making them harder to interpret. In particular, the free b_n s have a perfectly dimerized form for n > 3, and therefore a periodicity of 2. In contrast, the b_n s shown by the blue circles (Fig. 5(b-e)) have a longer periodicity, close to 3. The spectra for the spin basis are shown in Fig. 5(g-j) (blue circles). These spectra are not restricted to the FBZ. In addition, the periodicity of 3 manifests as 3 gaps for the spectra shown by the blue circles (Fig. 5(g-j)), with the gaps located at $\pm \pi$, 0. These gaps are most clearly visible for the smallest $J_z = 0.001$ (Fig. 5(g)). In contrast, the spectra of the free b_n s (Fig. 5(f)) have only two gaps. The additional gap in the spectra shown by the blue circles arises because the system has lost information that the quasienergy spectra are continuous with π being the same as $-\pi$.

One may map the dynamics to an alternate Krylov subspace using an Arnoldi iteration scheme [60] that works directly with the Floquet unitary, rather than its logarithm, and therefore bypasses some of the ambiguities of the Lanczos iteration. Alternatively, below we devise a scheme that can extract the relevant physics from Lanczos by a suitable gauge choice.

Since the spectra are periodic, a physically more suitable gauge choice for the Krylov Hamiltonian is the

one where the spectra are folded back to lie within the FBZ (orange crosses in Fig. 5(g-j)). This folding requires transforming the Krylov Hamiltonian $H_K \to U_K \hat{\epsilon}_{\text{FBZ}} U_K^{\dagger}$, where $\hat{\epsilon}_{\text{FBZ}}$ is a diagonal matrix where all the energies lie in the FBZ, and U_K is the unitary matrix that diagonalizes H_K before the folding. The folding procedure is non-local, and therefore gives a new Hamiltonian, which is no longer tri-diagonal. Therefore, a second Lanczos iteration is carried out to recover the tri-diagonal form, resulting in a new set of b_n s that are shown by orange crosses in Fig. 5(b-e). After this transformation, the new b_n s bear a closer resemblance to the b_n s of the free case, thus making them easier to interpret.

In comparison to the free case, one notices that a dimerization persists even with interactions, but is nonuniform, and gradually decreases into the bulk of the chain. This is visible in both gauges, i.e., blue circles and orange stars in Fig. 5(a-e). The larger J_z is, the more rapidly the dimerization decays into the chain. The contrast is most visible between $J_z = 0.001$ (Fig. 5(b)) and $J_z = 0.05$ (Fig. 5(e)). The region of the chain where there is no dimerization, represents a metallic state. Thus we have a spatially inhomogeneous system in the presence of J_z where a disordered insulating region (represented by spatially fluctuating but non-zero dimerization) is separated from a metallic bulk. An operator with weight in the metallic bulk will spread rapidly, and its autocorrelation function will decay to zero within a few drive cycles. The existence of the metal is the signature of bulk heating because the metal has no localized states. The emergence of the metal is especially clear after the folding procedure where the gaps at zero quasi-energy begin to fill up after the folding, compare folded spectra represented by orange stars with the unfolded spectra represented by blue circles in Fig. 5(g-j). Recall that for the free case the dimerization exists throughout the bulk. Thus the structure of the b_n s for $J_z \neq 0$ gives us evidence that a quasi-localized edge mode can exist despite bulk heating.

The above picture also clarifies how the ASPM acquires a lifetime. Essentially the edge mode is localized initially at the left end of the chain, and is separated by a finite region of dimerization from the metallic bulk. Therefore, it has a non-zero probability of tunneling into the metallic region. Below we estimate the lifetime of the ASPM by determining this tunneling probability.

In order to make the discussion more quantitative, in Fig. 6(a) we plot the dimerization, i.e., absolute value of the nearest-neighbor b_n s, $M(n) = b_{n+1} - b_n$, corresponding to the data represented by the orange stars of Fig. 5. We plot this quantity after performing a moving average over 4 sites, and denote it as $\langle |M(n)| \rangle_4$. (See Supplementary Note 2 and Supplementary Figure 1 for the data without the averaging, and with only 2-site averaging for comparison.) We note that $\langle |M(n)| \rangle_4$ does not change with J_z for the first couple of sites (provided $J_z < 0.05$), while away from the edge, $\langle |M(n)| \rangle_4$ decreases with n when $J_z \neq 0$. In contrast, $\langle |M(n)| \rangle_4$ stays constant for

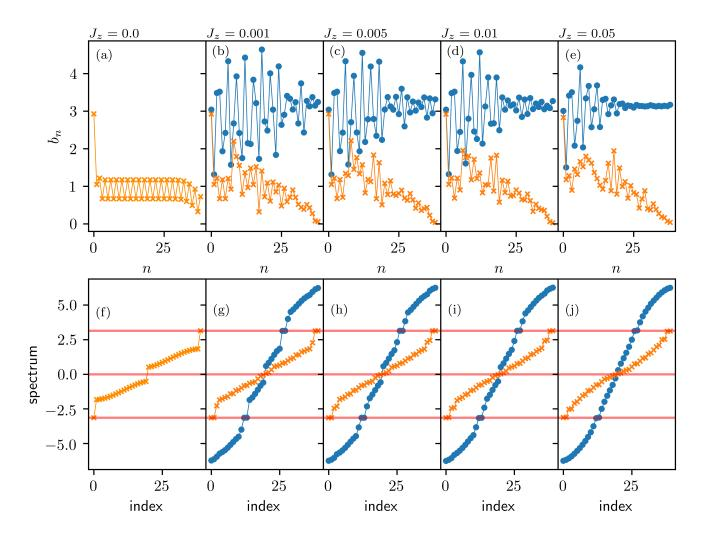


FIG. 5. Interaction dependence of the parameters of the Krylov chain. The Krylov chain hopping parameters b_n (panels (a-e)) and the corresponding spectra (panels (f-j)), where n labels the sites of the Krylov chain. The results are for a magnetic field of strength g = 0.3, period T = 8.25, and for the interaction J_z increasing from panels (a-e) and panels (f-j), with the $J_z = 0$ case shown in panels (a,f). The system size for $J_z = 0$ is L = 20 (same as Fig. 4), while that for the interacting cases is L = 12. Blue circles are for the unfolded spectra, while orange crosses for non-zero J_z are for a gauge choice where the spectra have been folded back into the Floquet Brillouin zone (FBZ). The folded spectra (orange crosses (g-j)), and the corresponding b_n (orange crosses (b-e)) bear a closer resemblance to the free problem (a,f). The horizontal red lines in panels (f-j) indicate energies at $0, \pm \pi$.

the free case. The fact that the first few sites of the Krylov chain do not change with J_z implies that H_E is not sensitive to J_z . We therefore adopt a simple model of a Krylov chain for the sites $n \geq 4$, with two slowly varying parameters, a nearest-neighbor average hopping $(b_n + b_{n-1})/2$, and the dimerization M(n) [46, 47] (see Supplementary Note 3).

We now emphasize some important differences between the b_n s for the ASZM in static systems [46, 47] and the same for the ASPM for Floquet systems. One is the sensitivity to gauge choice for the latter due to the freedom in shifting the quasi-energies by integer multiples of 2π (see detailed discussion above). The second difference is that when the Floquet spectrum is bounded by the FBZ, the average b_n s do not increase unboundedly with n, unlike in static systems. Thus we derive a continuum model under the assumption that the nearest-neighbor average hopping is spatially uniform, and that the dimerization is slowly varying in space. These assumptions map the Krylov chain onto a Dirac model with a spatially inhomogeneous mass (see Supplementary Note 3) $i\partial_t \tilde{\Psi} = [m(X)\sigma^y + \sigma^x i\partial_X] \tilde{\Psi}$, where m(n) = M(2n). For $J_z = 0$, the mass is spatially uniform and topologically non-trivial, m > 0, with M(2n) = -M(2n+1) = m. For $J_z \neq 0$, this mass vanishes into the bulk. While the precise model for how it vanishes is complicated, we adopt a simple ansatz where $m(X) = M_0\theta(X - X_0)$. Then a WKB treatment shows that the lifetime of the edge mode is (see Supplementary Note 3) $\Gamma \approx 4M_0e^{-2M_0X_0}$. The fact that the edge mode is at π energy rather than

at zero energy enters in the boundary condition via H_E , where a strong local hopping pins the edge mode to π .

We now discuss the J_z dependence of M_0 . Fig. 6(b) shows that $\langle |M(n=24)| \rangle_4 \sim J_z^{-1}$. Since the decay-rate Γ depends on the mass M_0 exponentially, and $M_0 \propto 1/J_z$, we conclude that $\Gamma \sim e^{-c/J_z}$.

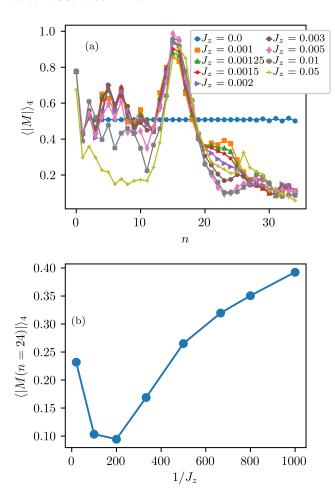


FIG. 6. Interaction dependence of the dimerization of the Krylov chain. The plot of the absolute value of the difference between neighboring Krylov hopping parameters b_n s, $M(n) = b_{n+1} - b_n$, after a moving average over four sites, and denoted as $\langle |M| \rangle_4$, where n labels the sites of the Krylov chain. Panel (a) shows how this quantity varies with n and interaction J_z . Panel (b) shows the variation with $1/J_z$ for this quantity at n = 24. This site is chosen because the interaction effects are the strongest here. Panel (b) indicates that the dimerization decays with interactions as $\langle |M(n = 24)| \rangle_4 \propto 1/J_z$ for $1/J_z \gg 1$.

Bound for lifetime from domain wall counting argument: We now present an alternate argument for the non-perturbatively long lifetime in Eq. (4). We show below that despite the low frequency driving, the energy required to flip the spin on the very first site is highly off-resonant, and requires rearranging many domain walls in the bulk. This phenomena was also noted in previous studies on static systems [42, 45, 46, 61]. Thus the boundary is in a prethermal state [62–66], despite the thermalized bulk. We argue this physics by deriving a Floquet Hamiltonian H_F in the limit of $J_z \ll 1$ and $|gT - \pi| \ll 1$. Recall $gT = \pi$ and $J_z = 0$ is the exactly solvable limit where the SPM is $\Psi_{\pi} = \sigma_1^x$.

Let us define $\hat{J}_z = J_z T/2, \hat{g} = Tg/2 - \pi/2$ and $\hat{J}_x = TJ_x/2$. We will work in the limit $\hat{J}_x \gg 1$ and $\hat{J}_z, \hat{g} \ll 1$. We cannot perform a high-frequency expansion [67] to construct H_F as \hat{J}_x is not small. Nevertheless, H_F to first order in \hat{J}_z, \hat{g} but to arbitrary orders in \hat{J}_x may be derived from an infinite resummation of the Baker-Campbell-Hausdorff formula [68, 69], leading to the following non-local perturbed Ising model [25]

$$TH_{F} \approx \hat{J}_{x}H_{xx} + \frac{\pi}{2}\mathcal{D} + \hat{g}\left\{h_{z}^{E}\hat{J}_{x}\cot(\hat{J}_{x}) + h_{z}^{B}\left(\frac{1+2\hat{J}_{x}\cot(2\hat{J}_{x})}{2}\right) + h_{xzx}\left(\frac{-1+2\hat{J}_{x}\cot(2\hat{J}_{x})}{2}\right) - \hat{J}_{x}\left(h_{xy} + h_{yx}\right)\right\} + \hat{J}_{z}\left\{h_{zz}^{E}\hat{J}_{x}\cot(\hat{J}_{x}) + h_{zz}^{B}\left(\frac{1+2\hat{J}_{x}\cot(2\hat{J}_{x})}{2}\right) - h_{xyyx}\left(\frac{-1+2\hat{J}_{x}\cot(2\hat{J}_{x})}{2}\right) + \hat{J}_{x}\left(h_{zyx} + h_{xyz}\right)\right\} + O(\hat{g}^{2}, \hat{J}_{z}^{2}).$$

$$(9)$$

Above $h_{\alpha_1...\alpha_k} = \sum_j \sigma_j^{\alpha_1} \dots \sigma_{j+k-1}^{\alpha_k} \equiv h_{\alpha_1...\alpha_k}^E + h_{\alpha_1...\alpha_k}^B$, where h^E denotes the contributions from the edge spins $\sigma_{1.L}^{\alpha}$ and h^B denotes the bulk spins.

Let us consider the energetics involved in flipping σ_1^x for $\hat{g} = \hat{J}_z = 0$. Since the boundary spin has only one neighbor, this flip costs energy \hat{J}_x . However, the energy cost for creating a domain wall in the bulk is $2\hat{J}_x$ due to the two neighboring sites. Thus there is a mismatch of $\hat{J}_x \gg 1$ between a bulk and an edge excitation, making the flipping of an edge spin impossible. However this simple argument does not account for processes that can make the domain wall hop from site to site, resulting in a lowering of its energy. Thus, we have to revisit the energy argument by accounting for the kinetic energy of the domain walls.

In order to develop our argument, we first note that H_{xx} counts the number of domain-walls $N = \sum_i \sigma_i^x \sigma_{i+1}^x$. Therefore, we write H_F as a part that commutes with the number of domain walls, and a part that changes the number of domain walls. In particular, $TH_F = \hat{J}_x N + D + V$ where [D, N] = 0 and $[V, N] \neq 0$. Both D and V can be written in the form similar to Eq. (9), i.e., as sums over local strings of Pauli matrices. The precise forms of D and V are not needed for our qualitative argument. We only assume that the operator norms of each of the local terms of D and V are $O(\hat{g}, \hat{J}_z)$. If these assumptions are valid we can apply the arguments of Refs. [42, 45, 46, 61] to find a lower bound on the lifetime of the ASPM. Here, we briefly summarize the physical picture.

First, consider the Hamiltonian \hat{J}_xN+D . The spectrum of the \hat{J}_x -term are states that are separated by multiples of \hat{J}_x because N counts domain walls. The D-term causes the domain walls to move without changing their number. Diagonalization of \hat{J}_xN+D results in domain wall "bands" with a typical bandwidth $\epsilon \sim ||D|| \sim O(\hat{g}, \hat{J}_z)$ which is much smaller than the separation \hat{J}_x between the bands.

The V-term of the total Hamiltonian does change the number of domain walls, but only by an even number due to the parity symmetry of the total Hamiltonian. A single application of V therefore changes the energy by about $2\hat{J}_x$ and is off resonant with the cost \hat{J}_x of flip-

ping the boundary spin. It is impossible to absorb the energy \hat{J}_x within few orders of perturbation theory in V. However, the creation and annihilation of a pair of domain walls would lead to the change of the energy by the order of the bandwidth $\epsilon \ll \hat{J}_x$. Therefore, we estimate that one needs of the order of J_x/ϵ powers of V to offset the energy \hat{J}_x required to flip a boundary spin. The probability corresponding to the required order of perturbation theory goes as $[||V||]^{\hat{J}_x/\epsilon} \sim [||V||]^{J_x/O(J_z,g)}$ where |V| denotes the typical size of the matrix element that creates a domain wall. The above expression is a lower bound for the lifetime. For example, in the two integrable limits (which is a property of the exact rather than the approximate H_F) $J_z \rightarrow 0, g \neq 0$ and $g \rightarrow 0, J_z \neq 0$, the lifetime should diverge. Empirically combining this observation with the rough estimate above we expect $1/\epsilon = O(1/J_z, 1/g)$. When $J_z \ll g$ this empirical formula replaces $\epsilon \to J_z$ in the above estimate making it consistent with Eq. (4).

Conclusions: ASPMs are fascinating objects which have lifetimes that far exceed bulk heating times. Besides presenting evidence for this, we developed a method for extracting their lifetimes by mapping their dynamics to single-particle quantum mechanics in Krylov subspace. While we studied the lifetime for $J_z \ll g$, determining the lifetime when g, J_z are comparable is left for future studies. Our Krylov method for determining lifetimes is generalizable to any spatial dimension, to closed and open systems, and to static and driven systems. In addition, the resistance to heating of the π mode is promising for its experimental realization [70].

Data Availability: All relevant data are available from the corresponding author upon reasonable request.

Author contributions: DJY and AM performed the numerical and analytical calculations. AGA and AM helped in the interpretation of the results and in the writing of the manuscript.

Competing Interests: The authors declare no competing interests.

Acknowledgements: This work was supported by the US Department of Energy, Office of Science, Basic Energy Sciences, under Award No. DE-SC0010821 (DJY and AM) and by the US National Science Foundation Grant NSF DMR-1606591 (AGA).

REFERENCES

- T. Oka and S. Kitamura, Floquet engineering of quantum materials, Annual Review of Condensed Matter Physics 10, 387 (2019), https://doi.org/10.1146/annurevconmatphys-031218-013423.
- [2] M. S. Rudner and N. H. Lindner, Band structure engineering and non-equilibrium dynamics in floquet topological insulators, Nat. Rev. Phys. 2, 229 (2020).
- [3] F. Harper, R. Roy, M. S. Rudner, and S. Sondhi, Topology and broken symmetry in floquet systems, Annual Review of Condensed Matter Physics 11, 345 (2020).
- [4] S. Ryu, A. P. Schnyder, A. Furusaki, and A. W. W. Ludwig, Topological insulators and superconductors: tenfold way and dimensional hierarchy, New Journal of Physics 12, 065010 (2010).
- [5] X.-L. Qi and S.-C. Zhang, Topological insulators and superconductors, Rev. Mod. Phys. 83, 1057 (2011).
- [6] B. A. Bernevig and (with T. L. Hughes), Topological Insulator and Topological Superconductors, Princeton University Press, Princeton (2013).
- [7] D. Carpentier, P. Delplace, M. Fruchart, and K. Gawedzki, Topological index for periodically driven time-reversal invariant 2d systems, Phys. Rev. Lett. 114, 106806 (2015).
- [8] R. Roy and F. Harper, Abelian floquet symmetryprotected topological phases in one dimension, Phys. Rev. B 94, 125105 (2016).
- [9] R. Roy and F. Harper, Periodic table for floquet topological insulators, Phys. Rev. B 96, 155118 (2017).
- [10] T. Kitagawa, E. Berg, M. Rudner, and E. Demler, Topological characterization of periodically driven quantum systems, Phys. Rev. B 82, 235114 (2010).
- [11] M. S. Rudner, N. H. Lindner, E. Berg, and M. Levin, Anomalous edge states and the bulk-edge correspondence for periodically driven two-dimensional systems, Phys. Rev. X 3, 031005 (2013).
- [12] F. Nathan, M. S. Rudner, N. H. Lindner, E. Berg, and G. Refael, Quantized magnetization density in periodically driven systems, Phys. Rev. Lett. 119, 186801 (2017).
- [13] P. Titum, E. Berg, M. S. Rudner, G. Refael, and N. H. Lindner, Anomalous floquet-anderson insulator as a nonadiabatic quantized charge pump, Phys. Rev. X 6, 021013 (2016).
- [14] L. Jiang, T. Kitagawa, J. Alicea, A. R. Akhmerov, D. Pekker, G. Refael, J. I. Cirac, E. Demler, M. D. Lukin, and P. Zoller, Majorana fermions in equilibrium and in driven cold-atom quantum wires, Phys. Rev. Lett. 106, 220402 (2011).
- [15] M. Thakurathi, A. A. Patel, D. Sen, and A. Dutta, Floquet generation of majorana end modes and topological invariants, Phys. Rev. B 88, 155133 (2013).
- [16] J. K. Asbóth, B. Tarasinski, and P. Delplace, Chiral symmetry and bulk-boundary correspondence in periodically driven one-dimensional systems, Phys. Rev. B 90, 125143 (2014).
- [17] K. Sacha and J. Zakrzewski, Time crystals: a review, Reports on Progress in Physics 81, 016401 (2017).
- [18] D. V. Else, C. Monroe, C. Nayak, and N. Y. Yao, Dis-

- crete time crystals, Annual Review of Condensed Matter Physics 11, 467 (2020).
- [19] V. Khemani, R. Moessner, and S. Sondhi, A brief history of time crystals, arXiv:1910.10745 (2019).
- [20] V. Khemani, A. Lazarides, R. Moessner, and S. L. Sondhi, Phase structure of driven quantum systems, Phys. Rev. Lett. 116, 250401 (2016).
- [21] C. W. von Keyserlingk, V. Khemani, and S. L. Sondhi, Absolute stability and spatiotemporal long-range order in floquet systems, Phys. Rev. B 94, 085112 (2016).
- [22] C. W. von Keyserlingk and S. L. Sondhi, Phase structure of one-dimensional interacting floquet systems. i. abelian symmetry-protected topological phases, Phys. Rev. B 93, 245145 (2016).
- [23] C. W. von Keyserlingk and S. L. Sondhi, Phase structure of one-dimensional interacting floquet systems. ii. symmetry-broken phases, Phys. Rev. B 93, 245146 (2016).
- [24] V. M. Bastidas, C. Emary, G. Schaller, and T. Brandes, Nonequilibrium quantum phase transitions in the ising model, Phys. Rev. A 86, 063627 (2012).
- [25] D. J. Yates, F. H. L. Essler, and A. Mitra, Almost strong $(0,\pi)$ edge modes in clean interacting one-dimensional floquet systems, Phys. Rev. B **99**, 205419 (2019).
- [26] G. J. Sreejith, A. Lazarides, and R. Moessner, Parafermion chain with $2\pi/k$ floquet edge modes, Phys. Rev. B **94**, 045127 (2016).
- [27] D. A. Huse, R. Nandkishore, and V. Oganesyan, Phenomenology of fully many-body-localized systems, Phys. Rev. B 90, 174202 (2014).
- [28] Y. Bahri, R. Ronen, and E. Altman, Localization and topology protected quantum coherence at the edge of hot matter, Nature Communications 6, 7341 (2015).
- [29] D. V. Else, B. Bauer, and C. Nayak, Floquet time crystals, Phys. Rev. Lett. 117, 090402 (2016).
- [30] I.-D. Potirniche, A. C. Potter, M. Schleier-Smith, A. Vishwanath, and N. Y. Yao, Floquet symmetryprotected topological phases in cold-atom systems, Phys. Rev. Lett. 119, 123601 (2017).
- [31] A. Kumar, P. T. Dumitrescu, and A. C. Potter, String order parameters for one-dimensional floquet symmetry protected topological phases, Phys. Rev. B 97, 224302 (2018).
- [32] T.-S. Zeng and D. N. Sheng, Prethermal time crystals in a one-dimensional periodically driven floquet system, Phys. Rev. B **96**, 094202 (2017).
- [33] A. Haldar, R. Moessner, and A. Das, Onset of floquet thermalization, Phys. Rev. B 97, 245122 (2018).
- [34] A. Haldar, D. Sen, R. Moessner, and A. Das, Dynamical freezing and scar points in strongly driven floquet matter: Resonance vs emergent conservation laws, Phys. Rev. X 11, 021008 (2021).
- [35] A. Chandran and S. L. Sondhi, Interaction-stabilized steady states in the driven o(n) model, Phys. Rev. B 93, 174305 (2016).
- [36] M. Natsheh, A. Gambassi, and A. Mitra, Critical properties of the floquet time crystal within the gaussian approximation, Phys. Rev. B 103, 014305 (2021).
- [37] M. Natsheh, A. Gambassi, and A. Mitra, Critical properties of the prethermal floquet time crystal, Phys. Rev. B 103, 224311 (2021).

- [38] A. Y. Kitaev, Unpaired majorana fermions in quantum wires, Physics-Uspekhi 44, 131 (2001).
- [39] P. Fendley, Parafermionic edge zero modes in z_n-invariant spin chains, Journal of Statistical Mechanics: Theory and Experiment 2012, P11020 (2012).
- [40] A. S. Jermyn, R. S. K. Mong, J. Alicea, and P. Fendley, Stability of zero modes in parafermion chains, Phys. Rev. B 90, 165106 (2014).
- [41] P. Fendley, Strong zero modes and eigenstate phase transitions in the xyz/interacting majorana chain, Journal of Physics A: Mathematical and Theoretical **49**, 30LT01 (2016).
- [42] D. V. Else, P. Fendley, J. Kemp, and C. Nayak, Prethermal strong zero modes and topological qubits, Phys. Rev. X 7, 041062 (2017).
- [43] J. Kemp, N. Y. Yao, C. R. Laumann, and P. Fendley, Long coherence times for edge spins, Journal of Statistical Mechanics: Theory and Experiment 2017, 063105 (2017).
- [44] D. E. Parker, R. Vasseur, and T. Scaffidi, Topologically protected long edge coherence times in symmetry-broken phases, Phys. Rev. Lett. 122, 240605 (2019).
- [45] J. Kemp, N. Y. Yao, and C. R. Laumann, Symmetryenhanced boundary qubits at infinite temperature, Phys. Rev. Lett. 125, 200506 (2020).
- [46] D. J. Yates, A. G. Abanov, and A. Mitra, Lifetime of almost strong edge-mode operators in one-dimensional, interacting, symmetry protected topological phases, Phys. Rev. Lett. 124, 206803 (2020).
- [47] D. J. Yates, A. G. Abanov, and A. Mitra, Dynamics of almost strong edge modes in spin chains away from integrability, Phys. Rev. B 102, 195419 (2020).
- [48] V. Vishwanath and G. Müller, The Recursion Method: Applications to Many-Body Dynamics, Springer, New York (2008).
- [49] A. Dymarsky and A. Gorsky, Quantum chaos as delocalization in krylov space, Phys. Rev. B 102, 085137 (2020).
- [50] A. Avdoshkin and A. Dymarsky, Euclidean operator growth and quantum chaos, Phys. Rev. Research 2, 043234 (2020).
- [51] H. Kim, T. N. Ikeda, and D. A. Huse, Testing whether all eigenstates obey the eigenstate thermalization hypothesis, Phys. Rev. E 90, 052105 (2014).
- [52] A. Lazarides, A. Das, and R. Moessner, Equilibrium states of generic quantum systems subject to periodic driving, Phys. Rev. E 90, 012110 (2014).
- [53] L. D'Alessio and M. Rigol, Long-time behavior of isolated periodically driven interacting lattice systems, Phys. Rev. X 4, 041048 (2014).
- [54] P. Ponte, A. Chandran, Z. Papić, and D. A. Abanin, Periodically driven ergodic and many-body localized quan-

- tum systems, Annals of Physics 353, 196 (2015).
- [55] M. Bukov, M. Heyl, D. A. Huse, and A. Polkovnikov, Heating and many-body resonances in a periodically driven two-band system, Phys. Rev. B 93, 155132 (2016).
- [56] D. E. Parker, X. Cao, A. Avdoshkin, T. Scaffidi, and E. Altman, A universal operator growth hypothesis, Phys. Rev. X 9, 041017 (2019).
- [57] J. Barbón, E. Rabinovici, R. Shir, and R. Sinha, On the evolution of operator complexity beyond scrambling, Journal of High Energy Physics 2019, 264 (2019).
- [58] W. P. Su, J. R. Schrieffer, and A. J. Heeger, Solitons in polyacetylene, Phys. Rev. Lett. 42, 1698 (1979).
- [59] W. P. Su, J. R. Schrieffer, and A. J. Heeger, Soliton excitations in polyacetylene, Phys. Rev. B 22, 2099 (1980).
- [60] W. E. Arnoldi, The principle of minimized iterations in the solution of the matrix eigenvalue problem, Quart. Appl. Math. 9, 17 (1951).
- [61] D. V. Else, B. Bauer, and C. Nayak, Prethermal phases of matter protected by time-translation symmetry, Phys. Rev. X 7, 011026 (2017).
- [62] D. A. Abanin, W. De Roeck, and F. Huveneers, Exponentially slow heating in periodically driven many-body systems, Phys. Rev. Lett. 115, 256803 (2015).
- [63] T. Kuwahara, T. Mori, and K. Saito, Floquet-magnus theory and generic transient dynamics in periodically driven many-body quantum systems, Annals of Physics 367, 96 (2016).
- [64] T. Mori, T. Kuwahara, and K. Saito, Rigorous bound on energy absorption and generic relaxation in periodically driven quantum systems, Phys. Rev. Lett. 116, 120401 (2016).
- [65] D. A. Abanin, W. De Roeck, W. W. Ho, and F. Huveneers, Effective hamiltonians, prethermalization, and slow energy absorption in periodically driven many-body systems, Phys. Rev. B 95, 014112 (2017).
- [66] D. Abanin, W. De Roeck, W. W. Ho, and F. Huveneers, A rigorous theory of many-body prethermalization for periodically driven and closed quantum systems, Communications in Mathematical Physics 354, 809 (2017).
- [67] A. Eckardt and E. Anisimovas, High-frequency approximation for periodically driven quantum systems from a floquet-space perspective, New Journal of Physics 17, 093039 (2015).
- [68] R. Scharf, The campbell-baker-hausdorff expansion for classical and quantum kicked dynamics, Journal of Physics A: Mathematical and General 21, 2007 (1988).
- [69] L. D'Alessio and A. Polkovnikov, Many-body energy localization transition in periodically driven systems, Annals of Physics 333, 19 (2013).
- [70] D. T. Liu, J. Shabani, and A. Mitra, Floquet majorana zero and π modes in planar josephson junctions, Phys. Rev. B **99**, 094303 (2019).

SUPPLEMENTARY NOTE 1: DERIVATION OF EQ. (8) AND THE CORRESPONDING KRYLOV HOPPING PARAMETERS

For the binary drive corresponding to setting $J_z = 0$ in Eq. (1) in the main text, it is convenient to map the problem to Majorana fermions as follows

$$a_{2\ell-1} = \prod_{j=1}^{\ell-1} \sigma_j^z \sigma_\ell^x; \ a_{2\ell} = \prod_{j=1}^{\ell-1} \sigma_j^z \sigma_\ell^y,$$
 (S1)

where $\ell = 1 \dots L$. Denoting the vector

$$\vec{a} = \begin{pmatrix} a_1 \\ a_2 \\ a_3 \\ \vdots \\ a_{2I} \end{pmatrix}, \tag{S2}$$

and for a system of size L, the time-evolution of an operator $\vec{a} = [a_1, a_2, a_3, \dots a_{2L}]^T$ is given by Eq. (7) in the main text. The explicit form for K for a system of size L = 3 is [25]

$$K = \begin{pmatrix} c_1 & -s_1 & 0 & 0 & 0 & 0 \\ s_1c_2 & c_1c_2 & -c_1s_2 & s_1s_2 & 0 & 0 \\ s_1s_2 & c_1s_2 & c_1c_2 & -s_1c_2 & 0 & 0 \\ 0 & 0 & s_1c_2 & c_1c_2 & -c_1s_2 & s_1s_2 \\ 0 & 0 & s_1s_2 & c_1s_2 & c_1c_2 & -s_1c_2 \\ 0 & 0 & 0 & 0 & s_1 & c_1 \end{pmatrix}.$$
(S3)

where,

$$c_1 = \cos(Tg),\tag{S4a}$$

$$c_2 = \cos(T),\tag{S4b}$$

$$s_1 = \sin(Tg),\tag{S4c}$$

$$s_2 = \sin(T). \tag{S4d}$$

K is a real orthogonal matrix as it represents rotations in the Majorana basis,

$$K^T K = 1. (S5)$$

K can be easily generalized to larger system sizes by noting that the second and third rows keep repeating (upto a shift by two columns to the right) until the last row i.e, the 2L-th row.

An exactly solvable point for the π modes is $Tg = \pi$ [20]. Denoting $K = K_0$ when $Tg = \pi$, and noting that at this point $s_1 = 0, c_1 = -1$, we have

For later use, we also write the inverse of K_0 explicitly,

$$K_0^{-1} = \begin{pmatrix} -1 & 0 & 0 & 0 & 0 & 0 \\ 0 & -c_2 & -s_2 & 0 & 0 & 0 \\ 0 & s_2 & -c_2 & 0 & 0 & 0 \\ 0 & 0 & 0 & -c_2 & -s_2 & 0 \\ 0 & 0 & 0 & s_2 & -c_2 & 0 \\ 0 & 0 & 0 & 0 & 0 & -1 \end{pmatrix}.$$
(S7)

Taking the logarithm of the above quantity, one obtains

$$\ln K_0 = -iT \begin{pmatrix} 0 & 0 & 0 & 0 & 0 & 0 \\ 0 & 0 & -i & 0 & 0 & 0 \\ 0 & i & 0 & 0 & 0 & 0 \\ 0 & 0 & 0 & 0 & -i & 0 \\ 0 & 0 & 0 & 0 & 0 & 0 \end{pmatrix} \pm i\pi.$$
(S8)

The first part of the equation hosts a zero mode, while the term $\pm \pi$ shifts the energy to $\pm \pi$, giving a strong π mode (SPM).

We now study the effect of small deviations from the exactly solvable limit $gT = \pi$. Let us write, $K = K_0 + V_p$ where

$$V_{p} = \begin{pmatrix} 0 & -s_{1} & 0 & 0 & 0 & 0\\ s_{1}c_{2} & 0 & 0 & s_{1}s_{2} & 0 & 0\\ s_{1}s_{2} & 0 & 0 & -s_{1}c_{2} & 0 & 0\\ 0 & 0 & s_{1}c_{2} & 0 & 0 & s_{1}s_{2}\\ 0 & 0 & s_{1}s_{2} & 0 & 0 & -s_{1}c_{2}\\ 0 & 0 & 0 & 0 & s_{1} & 0 \end{pmatrix} + O(s_{1}^{2}). \tag{S9}$$

If in addition to imposing $|s_1| \ll 1$, we also impose that $T \ll 1$ (or $|s_2| \ll 1$), then K_0 and V_p commute if terms of $O(s_1s_2), O(s_1^2), O(s_2^2)$ and higher are neglected. Recall that if A and B are two commuting matrices [A, B] = 0, then,

$$\ln\left(A+B\right) \approx \ln A + A^{-1}B + \dots \tag{S10}$$

Neglecting terms of $O(s_1s_2)$, $O(s_1^2)$, $O(s_2^2)$ and higher, we have two commuting matrices $A = K_0$, $B = V_p$. We can then use Eq. (S10) to obtain the following expression to first order in s_1 and T

$$i \ln K \approx \begin{pmatrix} 0 & is_1 & 0 & 0 & 0 & 0 \\ -is_1 & 0 & -iT & 0 & 0 & 0 \\ 0 & iT & 0 & is_1 & 0 & 0 \\ 0 & 0 & -is_1 & 0 & -iT & 0 \\ 0 & 0 & 0 & iT & 0 & is_1 \\ 0 & 0 & 0 & 0 & -is_1 & 0 \end{pmatrix} \pm \pi.$$
(S11)

The above is Eq. (8) of the main text.

We now carry out the Krylov procedure. We will show that the Liouvillian in the Krylov basis is a tridiagonal matrix of the form

$$\mathcal{L} = \begin{pmatrix} b_1 \\ b_1 & b_2 \\ b_2 & \ddots \\ & \ddots \end{pmatrix} \pm \pi. \tag{S12}$$

Without loss of generalization, let us choose the + sign in $\pm \pi$ in Eq. (S11), and also take $s_1 > 0$. The first operator is $\sigma_1^x = a_1$, which is represented by the vector,

$$|O_1\rangle = [1, 0, 0, 0, 0, 0]^T.$$
 (S13)

We generate the second operator, or vector as follows,

$$|O_2'\rangle = i \ln K |O_1\rangle = [\pi, -is_1, 0, 0, 0, 0]^T.$$
 (S14)

The diagonal term of the Liouvillian is

$$\alpha_1 = (O_1|i\ln K|O_1) = (O_1|O_2') = \pi.$$
 (S15)

Now we orthogonalize the state $|O'_2\rangle$ with respect to the previous state as follows,

$$|O_2'') = |O_2'') - \alpha_1|O_1| = [0, -is_1, 0, 0, 0, 0]^T.$$
(S16)

The first hopping term in the Liouvillian is

$$b_1 = \sqrt{(O_2''|O_2'')} = s_1, \tag{S17}$$

and normalizing the resulting state we obtain

$$|O_2| = |O_2''|/b_1 = [0, -i, 0, 0, 0, 0]^T.$$
 (S18)

Continuing this process, we generate the next state by the application of $i \ln K$ to the previous state,

$$|O_3'| = i \ln K |O_2|$$

= $[s_1, -i\pi, T, 0, 0, 0]^T$. (S19)

The diagonal term of the Liouvillian is

$$\alpha_2 = (O_2|i \ln K|O_2) = (O_2|O_3') = \pi,$$
(S20)

and orthogonalizing with respect to the previous two states, we obtain

$$|O_3'') = |O_3') - \alpha_2|O_2| - b_1|O_1| = [0, 0, T, 0, 0, 0]^T.$$
(S21)

Thus the second hopping term is

$$b_2 = \sqrt{(O_3''|O_3'')} = T, (S22)$$

and the new state after normalization is

$$|O_3\rangle = |O_3''\rangle/b_2 = [0, 0, 1, 0, 0, 0]^T.$$
 (S23)

Repeating the process,

$$|O_4') = i \ln K |O_3|$$

= $[0, -iT, \pi, -is_1, 0, 0, 0]^T$. (S24)

The diagonal term is

$$\alpha_3 = (O_3 | O_4') = \pi, \tag{S25}$$

and orthogonalizing with respect to $|O_{1,2,3}\rangle$ we have

$$|O_4'') = |O_4') - \alpha_3|O_3|O_3|O_2| = [0, 0, 0, -is_1, 0, 0]^T.$$
(S26)

Thus,

$$b_3 = \sqrt{(O_4''|O_4'')} = s_1, \tag{S27}$$

and

$$|O_4\rangle = |O_4''\rangle/b_3 = [0, 0, 0, -i, 0, 0]^T.$$
 (S28)

We now see a straightforward pattern emerge where $b_{\text{odd}} = |s_1|$, $b_{\text{even}} = T$, with diagonal terms $\alpha_i = \pi$. A zero mode exists for the topologically non-trivial dimerization $|s_1| < T$. Due to the π term along the diagonals, the energy of the mode is increased to π .

SUPPLEMENTARY NOTE 2: DIMERIZATION AND ITS MOVING AVERAGE

For the free case $(J_z = 0)$, the absolute value of the dimerization, defined as the absolute value of the difference between neighboring b_n s, $|M(n)| = |b_{n+1} - b_n|$, is constant after the first few sites. However when interactions are added, the dimerization fluctuates from site to site. To obtain a physically meaningful quantity, in the main text, we performed a four site moving average of the absolute value of the dimerization. Here, Supplementary Figure 1(a) shows how the absolute value of the dimerization behaves without any averaging, while Supplementary Figure 1(b) shows how this quantity behaves after a two site moving average. Note that the main features of the dimerization, namely that it is now non-zero only over a finite spatial region of size $n \approx 25$, beyond which it decays to zero, is preserved in the averaging procedure.

SUPPLEMENTARY NOTE 3: MAPPING TO A DIRAC MODEL WITH INHOMOGENEOUS MASS

The Schrödinger equation for the edge mode in Krylov subspace can be written as

$$i\partial_t \Psi_n = b_n \Psi_{n+1} + b_{n-1} \Psi_{n-1}. \tag{S29}$$

Note that we are considering a semi-infinite system where $n \ge 1$ with $b_0 = 0$. Since any diagonal term is a constant of the form integer $\times \pi$, we drop it here, as its effect would be to simply shift the energy of the edge mode by the constant amount.

To transform to the continuum limit we assume that the hopping parameters and the wavefunction can be written as

$$\Psi_n = i^n \left[\psi_n + (-1)^n \tilde{\psi}_n \right], \tag{S30}$$

$$b_n = h_n + (-1)^n \tilde{h}_n, \tag{S31}$$

where ψ_n , $\tilde{\psi}_n$, h_n , \tilde{h}_n are all assumed to be smooth, slowly varying functions of n. We now measure distances in lattice spacings x = n, introduce continuous notations $\psi_n = \psi(x)$ etc., and introduce the spinor,

$$\tilde{\Psi} = \begin{pmatrix} \psi(x) \\ \tilde{\psi}(x) \end{pmatrix}. \tag{S32}$$

In Eq. (S29) we substitute the ansatz Eq. (S30) for the wavefunction, and the ansatz Eq. (S31) for the hopping amplitudes. Following the derivation outlined in Ref. 47 which assumes that $h, \tilde{h}, \psi, \tilde{\psi}$ are smoothly varying functions of x, we arrive at,

$$i\partial_t \tilde{\Psi}(x) = [\sigma^y m(x) + \sigma^z \{ i\partial_x, h(x) \}] \tilde{\Psi}(x). \tag{S33}$$

Above, the mass is defined as

$$m(x) = 2\tilde{h}(x) - \partial_x \tilde{h}(x). \tag{S34}$$

An important difference between the static problem [47], and the Floquet problem studied here is that since the Floquet spectrum is bounded, the average of the nearest-neighbor hoppings, $h(x) \approx \text{constant}$. In the static case $h(x) \propto x$, and therefore grows unboundedly as x increases. Under the assumption of a constant h(x) = h, we arrive at,

$$i\partial_t \tilde{\Psi}(X,t) = \left[\sigma^z i\partial_X + \sigma^y m(X)\right] \tilde{\Psi}(X,t), \tag{S35}$$

where the mass is space dependent, and we defined a rescaled coordinate X = x/2h.

To capture the main physics of the non-perturbative effect of J_z , it is sufficient to make the assumption that $m(X) = M_0 = \text{const} > 0$ for $0 \le X \le X_0$ and m(X) = 0 for $X > X_0$. For this case, after a straightforwardly application of the WKB treatment, one finds the decay rate to be [47],

$$\Gamma \approx 4M_0 e^{-2M_0 X_0} \,. \tag{S36}$$

- 1

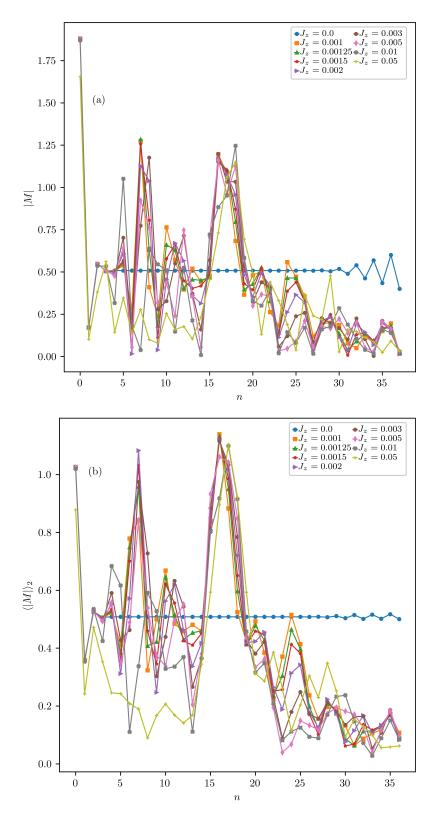


FIG. S1. Supplementary Figure 1: Absolute value of the dimerization and its moving average. Panel (a): The plot of the absolute value of the difference between neighboring b_n s, $|M(n)| = |b_{n+1} - b_n|$. Panel (b): The plot of the absolute value of the difference between neighboring b_n s, and averaged over 2 sites. This quantity is denoted as $\langle |M| \rangle_2$. The main text shows the same quantity, but after a 4-site averaging. One notes that when $J_z \neq 0$, |M| fluctuates with position n. However, it is non-zero upto about n = 25, beyond which it decays to zero. In addition, as J_z increases, the average dimerization decreases.